Published in IET Renewable Power Generation
Received on 24th December 2007
Revised on 18th March 2008
doi: 10.1049/iet-rpg:20070128

ISSN 1752-1416

Modelling adequacy of the doubly fed induction generator for small-signal stability studies in power systems

B.C. Pal F. Mei

Department of Electrical and Electronic Engineering, Imperial College London, SW7 2BT, UK
E-mail: b.pal@imperial.ac.uk

Abstract: The dynamics of the doubly fed induction generator (DFIG) with a closed-loop control is analysed. The analysis provides explanations of the impact of the closed-loop control on the DFIG dynamics and relevant modelling requirements for power system stability studies. The discussion considers generic PI controllers for the regulation of rotor speed, reactive power and pitch angle. It is shown that for the closed-loop-controlled DFIG, a simplified model, whereby both stator and rotor dynamics are neglected, is adequate. In such model, stator and rotor variables are algebraic, that is, they change instantaneously and the modelled dynamics are those of the controllers and mechanical parts. The observations and conclusions are obtained from eigenvalue, participation factor and time-domain analysis.

List of symbols and model parameters

ω_{el}	electrical base speed = $2\pi 50$, rad/s
ω_s	synchronous speed = 1 pu
ω_r, ω_t	rotor and turbine rotational speed
v_{qs}, v_{ds}	stator quadrature and direct voltage
v_{qr}, v_{dr}	rotor quadrature and direct voltage
i_{qs}, i_{ds}	stator quadrature and direct current
i_{qr}, i_{dr}	rotor quadrature and direct current
e'_{qs}, e'_{ds}	equivalent quadrature and direct voltage source behind transient impedance
θ_{tw}	shaft torsional angle (twist angle)
Φ_{iqr}, Φ_{idr}	state variable of inner loop controllers (current control)
Φ_{T_e}, Φ_{Q_s}	state variable of outer loop controllers (electrical torque and reactive power)
L_m	mutual inductance = 4 pu
L_{ss}	stator inductance = 1.01 L_m
L_{rr}	rotor inductance = 1.005 L_{ss}
K_{mrr}	$= L_m / L_{rr}$
L'_s	$= L_{ss} - L_m K_{mrr}$
R_s	stator resistance = 0.005 pu
R_r	rotor resistance = 1.1 R_s
R_1	$= R_s + R_2$
R_2	$= K^2_{mrr} R_r$
T_r	$= L_{rr}/R_r$
H_t	turbine inertia = 4 s
H_g	generator inertia = 0.1 H_t
k_{sh}	drive train shaft stiffness = 0.3 pu/el.rad
c_{sh}	drive train damping coefficient = 0.01 pu s/el.rad
P_{rated}	turbine rated power = 5 MW
v_{wrated}	rated wind speed = 12 m/s
$C_p(\lambda, \beta)$	coefficient of performance $= c_1c_2/(\lambda + c_8\beta) - c_2c_9/(\beta^3 + 1) - c_3\beta - c_4\beta^{c_5} - c_6 \exp(-c_7/(\lambda + c_8\beta)) + c_{10}\lambda$, where $c_1 = 0.22$, $c_2 = 116$, $c_3 = 0.4$, $c_4 = c_5 = 0$, $c_6 = 5$, $c_7 = 12.5$, $c_8 = 0.08$, $c_9 = 0.035$, $c_{10} = 0$ [7]
R	blade length = sqrt($P_{rated}/\{0.5\rho\pi C_{pmax} v^3_{wrated}\}$) = 58.6 m
ρ	air density = 1.225 kg/m^3
K_{opt}	$= 0.5\rho\pi R^5 C_{pmax} \omega^3_{tB}/(\lambda^3_{opt} P_{rated}) = 0.5787$

1 Introduction

The doubly fed induction generator (DFIG) is one of the preferred technologies in wind generation applications as it can operate over a wide range of rotor speeds [1–4]. The advantages are reduced mechanical stress and optimised power capture. Speed variability is possible due to the AC–DC–AC converter in the rotor circuit required to produce rotor voltage at slip frequency. Using a back-to-back converter allows bidirectional power flows and hence operation at both sub- and super-synchronous speed. Formulating the control algorithm of the converters in a synchronously rotating frame allows for effective control of the generator speed (or active power) and terminal voltage (or reactive power).

With increasing contribution from the asynchronous wind generations, there is a genuine concern that the dynamic characteristic and performance of the overall system needs proper investigation. Of particular interest is the small-signal stability performance of the system following the recovery from a large disturbance. One relevant question is whether the standard framework of multi-machine stability in interconnected system such as eigen value analysis can be extended to a system with asynchronous generation technology such as DFIG. If yes, what modelling complexity would be adequate to include DFIG into standard small-signal stability analysis tools? To investigate this, mathematical models are required. Depending on the point of interest, it is always useful to have specific and just adequate modelling information. Recent research [5, 6] suggests that for power system stability studies involving DFIG, it is common to ignore:

- the effect of stator transients (i.e. assume that the stator variables change instantaneously);
- the effect of converter switching (i.e. assume that the converters are sinusoidal voltage or current sources);
- the effect of the DC-link dynamics (i.e. assume that the DC-link voltage is constant with instantaneous active power transfer between the DFIG rotor and external grid).

More recently [7, 8], it has also been suggested that since rotor converter controls act very fast, an additional assumption can be made for power system studies, which is to neglect the effect of rotor electrical transients (i.e. assume that the rotor electrical variables change instantaneously).

In the latter modelling framework whereby both stator and rotor electrical transients are neglected, the DFIG is considered as a controlled electrical torque and reactive power source [7, 8]. Miller *et al.* [8] only report the time-domain results without detail description of the modelling framework.

This paper systematically introduces the modelling details and through system theory tool, such as eigenvalue analysis, it shows the relevance of various component models for low-frequency electromechanical oscillations analysis. It suggests the required model simplification following participation factor analysis of various component dynamics. The above simplifications are desirable in large-scale power system studies as they reduce the model order and hence are easily adaptable to standard simulation platform. It is shown that both the DFIG stator and rotor electrical transients can be neglected for stability studies. The approach taken is to compare the small-signal behaviour of the DFIG and squirrel-cage induction generator (SCIG). The change in dynamics due to closed-loop control justifies the appropriate modelling requirements.

The rest of the paper is organised as follows. In Section 2, the dynamical behaviour of the SCIG is presented. The modelling of DFIG and rotor-side converter power/voltage controller and pitch control mechanism are described. Time-domain response of the nonlinear model for the full-order model (with stator transients) and simplified models (without stator and rotor electrical transients) are compared. In Section 3, the dynamical behaviour of the closed-loop controlled DFIG is analysed. The impacts of the closed-loop controls are identified from the differences with respect to the SCIG. Section 4 discusses the observations and concludes the paper.

The DFIG model considered in the present paper assumes an algebraic mechanical power (turbine power) model, two-mass drive train, rotor-side converter as a controlled voltage source and grid-side converter as a controlled current source. More details are given in [9, 10]. Explanations through eigenvalue analysis [11, 12] and detailed results for the open-loop controlled case (DFIG with rotor voltage kept constant at some non-zero values) can also be found in [9, 10, 13, 14]. Symbols and parameters of the DFIG system are shown in Figs. 1 and 2.

2 Modelling

The dynamics of DFIG spans over a wide time scale. The pitch control with dead band and rate limits is quite slow because of larger inertia of the blade. The time constants

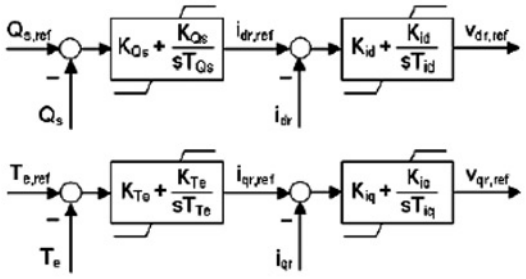

Figure 1 *Generic control loops of the DFIG rotor-side converter*

doi: 10.1049/iet-rpg:20070128

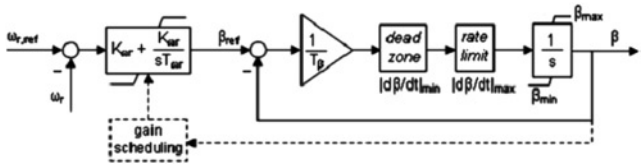

Figure 2 *Pitch controller and actuator*

are usually few seconds, making the frequency response of the dynamics relevant in the range of a tenth of Hz (0.1 Hz maximum). The fault response of the converter and associated converter protection circuits (such as crow bar) falls in fast transient regime (few milliseconds or hundreds of Hz). The consideration of these two together does not help to establish the role of DFIG in small-signal electromechanical oscillation stability assessment which has been the focus of the paper. On the other hand, their role in the respective time frame is important for the overall stability of the system. The motivation comes from a general concern of low frequency (0.2–2.0 Hz) electromechanical performance of interconnected power system that survives large disturbance but oscillates to reach post-disturbance acceptable equilibrium.

The modelling methodology is similar to standard d–q axes representation of induction generator.

The following set of differential algebraic equations is used for the DFIG. More details are in [10, 13, 14].

$$\frac{\mathrm{d}i_{\mathrm{qs}}}{\mathrm{d}t} = \frac{\omega_{\mathrm{el}}}{L'_{\mathrm{s}}}\left(-R_1 i_{\mathrm{qs}} + \omega_{\mathrm{s}} L'_{\mathrm{s}} i_{\mathrm{ds}} + \frac{\omega_{\mathrm{r}}}{\omega_{\mathrm{s}}} e'_{\mathrm{qs}} - \frac{1}{T_{\mathrm{r}}\omega_{\mathrm{s}}} e'_{\mathrm{ds}} - v_{\mathrm{qs}} + K_{\mathrm{mrr}} v_{\mathrm{qr}}\right) \tag{1}$$

$$\frac{\mathrm{d}i_{\mathrm{ds}}}{\mathrm{d}t} = \frac{\omega_{\mathrm{el}}}{L'_{\mathrm{s}}}\left(-\omega_{\mathrm{s}} L'_{\mathrm{s}} i_{\mathrm{qs}} - R_1 i_{\mathrm{ds}} + \frac{1}{T_{\mathrm{r}}\omega_{\mathrm{s}}} e'_{\mathrm{qs}} + \frac{\omega_{\mathrm{r}}}{\omega_{\mathrm{s}}} e'_{\mathrm{ds}} - v_{\mathrm{ds}} + K_{\mathrm{mrr}} v_{\mathrm{dr}}\right) \tag{2}$$

$$\frac{\mathrm{d}e'_{\mathrm{qs}}}{\mathrm{d}t} = \omega_{\mathrm{el}}\omega_{\mathrm{s}}\left(R_2 i_{\mathrm{ds}} - \frac{e'_{\mathrm{qs}}}{T_{\mathrm{r}}\omega_{\mathrm{s}}} + \left(1 - \frac{\omega_{\mathrm{r}}}{\omega_{\mathrm{s}}}\right) e'_{\mathrm{ds}} - K_{\mathrm{mrr}} v_{\mathrm{dr}}\right) \tag{3}$$

$$\frac{\mathrm{d}e'_{\mathrm{ds}}}{\mathrm{d}t} = \omega_{\mathrm{el}}\omega_{\mathrm{s}}\left(-R_2 i_{\mathrm{ds}} - \left(1 - \frac{\omega_{\mathrm{r}}}{\omega_{\mathrm{s}}}\right) e'_{\mathrm{qs}} - \frac{e'_{\mathrm{ds}}}{T_{\mathrm{r}}\omega_{\mathrm{s}}} + K_{\mathrm{mrr}} v_{\mathrm{qr}}\right) \tag{4}$$

$$\frac{\mathrm{d}\omega_{\mathrm{r}}}{\mathrm{d}t} = \frac{1}{2H_g}(k_{\mathrm{sh}}\theta_{\mathrm{tw}} + c_{\mathrm{sh}}\omega_{\mathrm{el}}(\omega_{\mathrm{t}} - \omega_{\mathrm{r}}) - T_{\mathrm{e}}) \tag{5}$$

$$\frac{\mathrm{d}\theta_{\mathrm{tw}}}{\mathrm{d}t} = \omega_{\mathrm{el}}(\omega_t - \omega_{\mathrm{r}}) \tag{6}$$

$$\frac{\mathrm{d}\omega_{\mathrm{t}}}{\mathrm{d}t} = \frac{1}{2H_t}(T_{\mathrm{m}} - k_{\mathrm{sh}}\theta_{\mathrm{tw}} - c_{\mathrm{sh}}\omega_{\mathrm{el}}(\omega_{\mathrm{t}} - \omega_{\mathrm{r}})) \tag{7}$$

$$0 = \sum_{k=1}^{n} V_i V_k Y_{ik} \cos(\theta_i - \theta_k - \alpha_{ik}) - P_{\mathrm{tot}} \tag{8}$$

$$0 = \sum_{k=1}^{n} V_i V_k Y_{ik} \sin(\theta_i - \theta_k - \alpha_{ik}) - Q_{\mathrm{tot}} \tag{9}$$

Equations (1) and (2) represent the stator electrical dynamics. They are obtained from the three-phase voltage equations of the induction machine, which are transformed into a synchronously rotating two-axis frame [2, 4]. The rotating frame (d–q-axes) can be aligned with any synchronously rotating variable such as the terminal voltage or stator flux. In the latter case, the control algorithm is similar to that of the vector control used in variable speed drive applications (induction motors). In this paper, the q-axis is aligned with stator voltage and the d-axis is leading the q-axis; hence $V_{\mathrm{s}} = v_{\mathrm{qs}} + jv_{\mathrm{ds}}$ and $v_{\mathrm{qs}} = |V_{\mathrm{s}}|$, $v_{\mathrm{ds}} = 0$.

If stator transients are neglected, the derivative terms in (1) and (2) are zero. Similarly, if rotor electrical transients are neglected, the derivative terms in (3) and (4) are zero. Equations (5)–(7) represent the drive train two-mass model, where ω_{r}, θ_{tw} and ω_{t} are the generator speed, shaft equivalent torsional angle and turbine speed, respectively. The electromagnetic torque T_{e} and mechanical torque T_{m} are

$$T_{\mathrm{e}} = \left(\frac{e'_{\mathrm{qs}}}{\omega_{\mathrm{s}}}\right) i_{\mathrm{qs}} + (e'_{\mathrm{ds}}/\omega_{\mathrm{s}}) i_{\mathrm{ds}} \tag{10}$$

$$T_{\mathrm{m}} = \left(\frac{0.5\rho\pi R^2 C_{\mathrm{p}}(\lambda, \beta) v_{\mathrm{w}}^3}{\omega_{\mathrm{t}}}\right)\left(\frac{1}{T_{\mathrm{mBase}}}\right) \tag{11}$$

where $C_{\mathrm{p}}(\lambda, \beta)$ is the turbine performance coefficient. The expression for C_{p} and other parameters are given in the list of symbols. Equations (8) and (9) are the algebraic equations representing the interface with the power system. The parameters Y_{ik} and α_{ik} are the magnitude and angle of the element (i, k) of the bus admittance matrix [11]. The variables V_i and θ_i are the magnitude and angle of the voltage at bus i. The total active and reactive power delivered to the grid are

$$P_{\mathrm{tot}} = P_{\mathrm{s}} + P_{\mathrm{GSC}} = v_{\mathrm{qs}} i_{\mathrm{qs}} + v_{\mathrm{ds}} i_{\mathrm{ds}} + P_{\mathrm{GSC}} \tag{12}$$

$$Q_{\mathrm{tot}} = Q_{\mathrm{s}} + Q_{\mathrm{GSC}} = -v_{\mathrm{qs}} i_{\mathrm{ds}} + v_{\mathrm{ds}} i_{\mathrm{qs}} + Q_{\mathrm{GSC}} \tag{13}$$

where P_{s} and Q_{s} are the stator active and reactive power.

The converters are very sensitive to high fault current and usually they are turned off fast through current-limited control during the situation of large current (fault). The rotor accelerates and produces higher voltage and current. Usually, this is addressed by crow-bar-type special protection where the rotor excessive energy is allowed to bypass the converter through crow bar protection. The dynamics associated with protection and converter

switching is fast and they can be easily represented in an EMTDC PSCAD environment. However, the protection and switching logics are generally assumed to be neglected for low-frequency small-signal stability studies. When the DC-link dynamics are also ignored, the model of the GSC is included in (8) and (9) since $P_{GSC} = P_r = v_{qr} i_{qr} + v_{dr} i_{dr}$ and $Q_{GSC} = \alpha Q_{tot}$, where α defines the reactive power sharing between stator and GSC. For minimum converter current rating as assumed in this paper, no sharing is done (i.e. the GSC is operated at unity power factor); hence $\alpha = 0$, $Q_{GSC} = 0$ and $Q_{tot} = Q_s$. The RSC is modelled as a controlled voltage source, which is described next.

The generic speed, power factor and pitch angle control loops are shown in Figs. 1 and 2. The reference reactive power is a constant determined by the wind farm control centre or a variable determined by an additional outer voltage control loop. In sub-rated wind speed, the reference torque is $T_{e,ref} = K_{opt}\,\omega_r^2$, where K_{opt} is a constant (defined below). The set of differential and algebraic equations (DAEs) of the controllers in Figs. 1 and 2 are written as

$$\frac{d\Phi_{T_e}}{dt} = T_{e,err} \tag{14}$$

$$\frac{d\Phi_{iq}}{dt} = K_{T_e} T_{e,err} + \frac{K_{T_e}}{T_{T_e}} \Phi_{T_e} - i_{qr} \tag{15}$$

$$v_{qr} = K_{iq} K_{T_e} T_{e,err} + K_{iq} \frac{K_{T_e}}{T_{T_e}} \Phi_{T_e} - K_{iq} i_{qr} + \frac{K_{iq}}{T_{iq}} \Phi_{iq} \tag{16}$$

$$\frac{d\Phi_{Q_s}}{dt} = Q_{s,err} \tag{17}$$

$$\frac{d\Phi_{id}}{dt} = K_{Q_s} Q_{s,err} + \frac{K_{Q_s}}{T_{Q_s}} \Phi_{Q_s} - i_{dr} \tag{18}$$

$$v_{dr} = K_{id} K_{Q_s} Q_{s,err} + K_{id} \frac{K_{Q_s}}{T_{Q_s}} \Phi_{Q_s} - K_{id} i_{dr} + \frac{K_{id}}{T_{id}} \Phi_{id} \tag{19}$$

$$\frac{d\Phi_{\omega_r}}{dt} = -\frac{1}{T_{\omega_r}} \Phi_{\omega_r} + \frac{1}{K_{\omega_r}} \beta_{ref} \tag{20}$$

$$\frac{d\beta}{dt} = \frac{1}{T_\beta} (\beta_{ref} - \beta) \tag{21}$$

$$\beta_{ref} = (\omega_{r,ref} - \omega_r) K_{\omega_r} + \Phi_{\omega_r} \frac{K_{\omega_r}}{T_{\omega_r}} \tag{22}$$

Equations (14)–(16) represent the q-axis control loop, $T_{e,err} = T_{e,ref} - T_e$ is the torque error, Φ_{T_e} the state variable of the outer controller and Φ_{iq} the state variable of the inner controller. Similarly, (17)–(19) represent the d-axis control loop, Φ_{Q_s} and Φ_{id} are the state variables of the outer and inner controllers respectively, $Q_{s,err} = Q_{s,ref} - Q_s$ is the reactive power output error. The parameters K_{iq}, K_{id}, K_{T_e} and K_{Q_s} are the controller proportional gains (P-gains). From Fig. 1, K_{iq} and K_{id} have units of impedance, K_{T_e} has units of speed over voltage and K_{Q_s} has units of voltage inversed. Below, their values are given in per-unit on machine base. The parameters T_{iq}, T_{id}, T_{T_e} and T_{Q_s} are the controller reset times or integral times and have units of second. Equations (20)–(22) are the DAEs for the pitch control. The parameters Φ_{ω_r}, K_{ω_r} and T_{ω_r} are, respectively, the state variable, proportional gain and integral time constant of the PI-controller, T_β the time constant of the actuators, β_{ref} and $\omega_{r,ref}$ the pitch angle and rotor speed set points.

Before analysing the closed-loop controlled DFIG, the dynamical characteristic of the SCIG, whereby rotor voltages are zero, is briefly discussed. Fig. 3 shows the response of the electrical torque and rotor speed to a 50% drop in terminal voltage for 100 ms following which the voltage recovers to nominal range. The response is shown for the full-order model, the model with stator transients neglected and the model with stator and rotor transients neglected. It is seen that simplifying the model by neglecting the electrical transients gives significantly different dynamical behaviour. For the full-order model, following the electrical disturbance, the dynamical response consists of a superposition of a high-frequency mode at about 50 Hz and a medium frequency mode at about

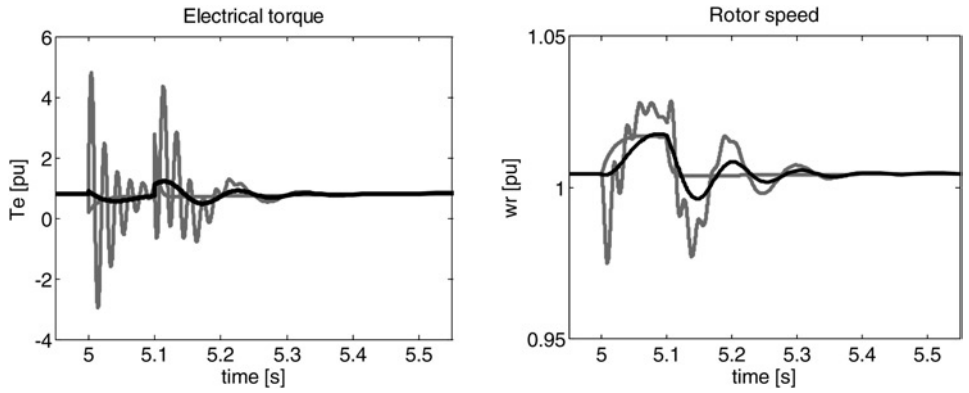

Figure 3 *SCIG: response of the electrical torque and rotor speed to drop in terminal voltage during 100 ms*
Dotted grey, full-order model; dash-dotted black, stator transients neglected; continuous grey, stator and rotor transients neglected

doi: 10.1049/iet-rpg:20070128

Table 1 Eigenvalues and participation factors obtained by linearising the SCIG model

$\lambda = \sigma \pm j\omega$	f, Hz	ζ	Dominant states (contribution in %)	
full-order model				
−16.46 ±j321.13	51.11	0.051	stator electrical	$i_{qs} = 48$, $i_{ds} = 46$
−10.15 ±j62.72	9.98	0.160	rotor electromechanical	$e'_{ds} = 48$, $\omega_r = 47$
−0.467 ±j3.33	0.530	0.139	turbine mechanical	$\theta_{tw} = 49$, $\omega_t = 50$
− 16.42	0	1	rotor electrical	$e'_{qs} = 99$
stator transients neglected				
−10.91 ±j62.11	9.88	0.173	rotor electromechanical	$e'_{ds} = 49$, $\omega_r = 49$
−0.467 ±j3.33	0.530	0.139	turbine mechanical	$\theta_{tw} = 49$, $\omega_t = 50$
−16.46	0	1	rotor electrical	$e'_{qs} = 99$
stator and rotor transients neglected				
−0.484 ±j3.38	0.538	0.142	turbine mechanical	$\theta_{tw} = 50$, $\omega_t = 50$
−225.00	0	1	rotor electrical	$e'_{qs} = 99$

λ, eigenvalues; f, oscillation frequency; ζ, damping ratio. Operating point: $\omega_r = 1.00452$ pu, $V_s = 1$ pu, $V_{qr} = 0$ pu, $V_{dr} = 0$ pu

10 Hz. Neglecting the stator transients gives a response without the 50 Hz oscillations and with smaller amplitudes for the 10 Hz mode. Neglecting the stator and rotor transients gives a response without oscillations.

The approximation of these dynamical characteristics can be obtained from the eigenvalues of the linearised SCIG model. Table 1 shows the eigenvalues and participation factors obtained by linearising the SCIG model around the operating point $V_s = 1$ pu, $\omega_r = 1.00452$ pu. From the participation factors of the dominant state variables (contribution in percent), it is seen that the high-frequency mode is the most sensitive to the stator electrical dynamics. The medium-frequency mode is the mainly associated with the rotor electrical and mechanical dynamics. Table 1 also shows that there is a low-frequency mode at about 0.5 Hz associated with the mechanical dynamics of the turbine. This mode is excited by mechanical disturbances, as shown in Fig. 4.

3 DFIG with closed-loop control

Fig. 5 shows schematically the closed-loop controlled DFIG. In this configuration, the rotor voltages and pitch angle are determined as a function of the operating point and desired level of power factor (or terminal voltage or reactive power) and active power (or rotor speed or electrical torque).

3.1 Dynamics at sub-synchronous speed

Fig. 6 shows the response of the electrical torque and rotor speed to a drop in terminal voltage during 100 ms for the DFIG operating at sub-synchronous speed. The response is shown for the full-order model, the model with stator

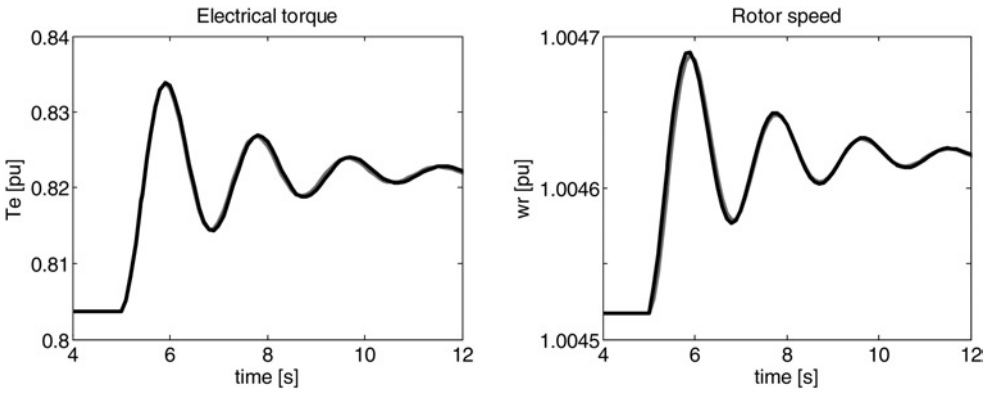

Figure 4 *SCIG: response of the electrical torque and rotor speed to 0.1 m/s step increase in wind speed*
Dotted grey, full-order model; dash-dotted black, stator transients neglected; continuous grey, stator and rotor transients neglected

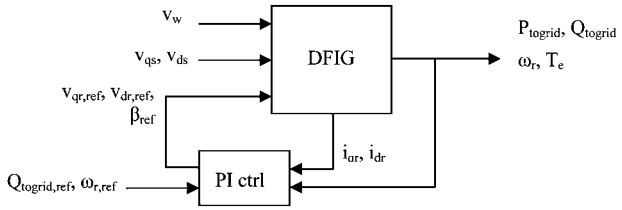

Figure 5 *Closed-loop controlled DFIGr*

transients neglected and the model with stator and rotor transients neglected. In contrast to the SCIG case in the previous section, it is seen that solely neglecting the stator transients does not remove the 50 Hz mode. For the closed-loop controlled DFIG, the high-frequency mode is removed when both stator and rotor electrical transients are neglected. In addition, as opposed to the SCIG situation, the simplified model is more conservative in the sense that rotor speed deviation is slightly larger when electrical transients are neglected.

These changes in dynamics can also be observed in the eigenvalues and participation factors shown in Table 2. It is seen that with the closed-loop control, the stator dynamics is associated with real pole far in the left-half plane, whereas the 50 Hz mode is mainly due to the rotor electrical dynamics. For the closed-loop control configuration, the full-order model has only two oscillatory modes as shown in Table 2: a 50 Hz electrical mode and a low-frequency mechanical mode, which is oscillating at 1.5 Hz for the machine parameters given in the list of symbols. The mechanical dynamics is not significantly coupled with the electrical ones. Neglecting the electrical transients does not impact the mechanical modes and controller modes significantly as shown in Table 2. As was observed in Fig. 6, Table 2 shows that for the model without stator transient there is a 50 Hz electrical mode.

3.2 Dynamics at synchronous speed

Fig. 7 shows the response of the electrical torque and rotor speed to a drop in terminal voltage during 100 ms for the DFIG operating at synchronous speed. The same observations can be made as in the previous section. Table 3 shows the corresponding eigenvalues and dominant states. As opposed to the open-loop case [10, 13, 14], the dynamical characteristics for the closed-loop control case are not significantly changed for operation at large positive slip (sub synchronous) or zero slip (synchronous speed).

3.3 Dynamics at super-synchronous speed

Fig. 8 shows the response of the electrical torque and rotor speed to a drop in terminal voltage during 100 ms for the DFIG operating at super-synchronous speed. The same observations can be made as in the previous section. Table 4 shows the corresponding eigenvalues and dominant states. The turbine mechanical mode is changed due to the additional pitching dynamics as the pitch control is activated in the higher rotor speed region. The electrical dynamics and the mechanical oscillations associated with rotor mechanical dynamics are not significantly different from the sub-synchronous and synchronous cases discussed in Sections 3.1 and 3.2.

4 Conclusion

In this paper, the dynamical behaviour of the DFIG is analysed for operation at sub-synchronous, synchronous and super-synchronous rotor speeds. Eigenvalues of SCIG and DFIG configurations are compared to identify the impacts of the closed-loop controls on the modelling adequacy.

For the SCIG, there are three oscillating modes. The high-frequency mode (50 Hz) is an electrical mode

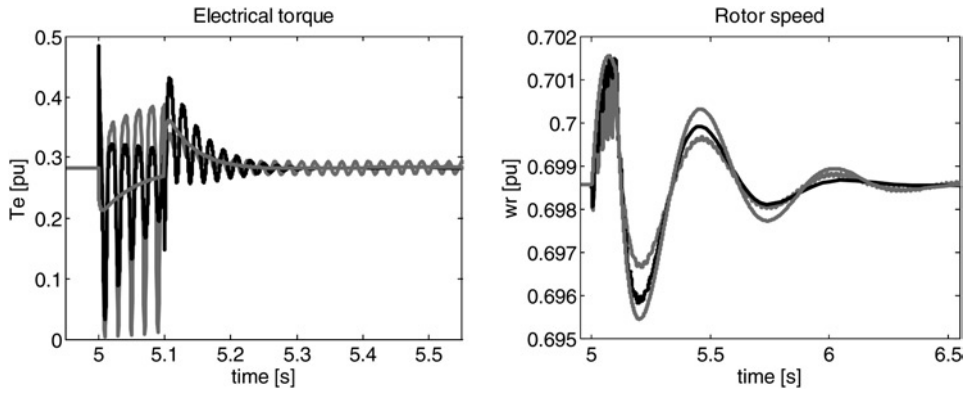

Figure 6 *Closed-loop DFIG at sub-synchronous speed: response of the electrical torque and rotor speed to a drop in terminal voltage during 100 ms*
Dotted grey, full-order model; dash-dotted black, stator transients neglected; continuous grey, stator and rotor transients neglected

doi: 10.1049/iet-rpg:20070128

Table 2 Closed-loop controlled DFIG at subsynchronous speed

$\lambda = \sigma \pm j\omega$	f, Hz	ζ	Dominant states (contribution in %)	
full-order model				
−7412.2	0	1	stator electrical	$i_{qs} = 93$
−2944.0	0	1	stator electrical	$i_{ds} = 91$
−0.232 ± j313.66	49.92	0.001	rotor electrical	$e'_{qs} = 49$, $e'_{ds} = 48$
−2.62 ± j11.17	1.78	0.228	rotor mechanical	$\omega_r = 46$, $\theta_{tw} = 49$
−0.138	0	1	turbine mechanical	$\omega_t = 91$, $\omega_r = 9$
−422.55	0	1	q-axis current control	$\Phi_{iqr} = 93$
−213.99	0	1	d-axis current control	$\Phi_{idr} = 92$
−23.50	0	1	torque control	$\Phi_{T_e} = 98$
−9.95	0	1	reactive power control	$\Phi_{qs} = 99$
stator transients neglected				
−6.64 ± j309.47	49.25	0.021	rotor electrical	$e'_{qs} = 49$, $e'_{ds} = 48$
−2.62 ± j11.17	1.78	0.228	rotor mechanical	$\omega_r = 46$, $\theta_{tw} = 49$
−0.138	0	1	turbine mechanical	$\omega_t = 91$, $\omega_r = 9$
−402.68	0	1	q-axis current control	$\Phi_{iqr} = 98$
−205.99	0	1	d-axis current control	$\Phi_{idr} = 96$
−23.52	0	1	torque control	$\Phi_{T_e} = 98$
−9.95	0	1	reactive power control	$\Phi_{qs} = 99$
stator and rotor transients neglected				
−2.62 ± j11.17	1.78	0.228	rotor mechanical	$\omega_r = 46$, $\theta_{tw} = 49$
−0.138	0	1	turbine mechanical	$\omega_t = 91$, $\omega_r = 9$
−399.02	0	1	q-axis current control	$\Phi_{iqr} = 99$
−198.61	0	1	d-axis current control	$\Phi_{idr} = 99$
−23.50	0	1	torque control	$\Phi_{T_e} = 98$
−9.95	0	1	reactive power control	$\Phi_{qs} = 99$

λ, eigenvalues; f, oscillation frequency; ζ, damping ratio. Operating point: $\omega_r = 0.7$ pu, $V_s = 1$ pu

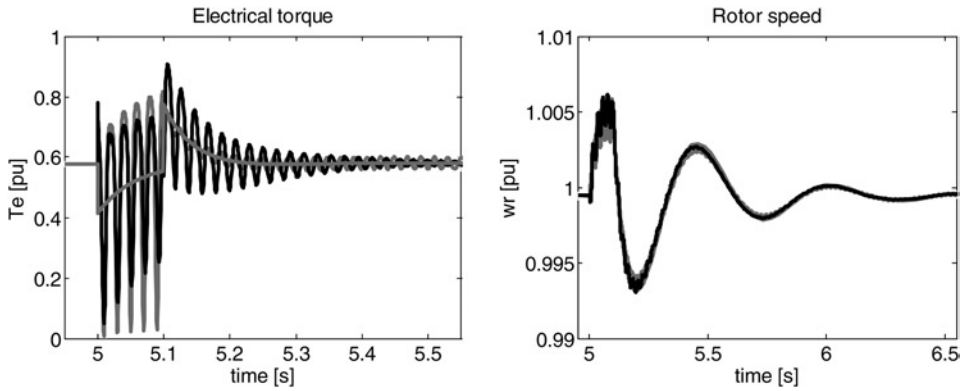

Figure 7 *Closed-loop DFIG at synchronous speed: response of the electrical torque and rotor speed to a drop in terminal voltage during 100 ms*
Dotted grey, full-order model; dash-dotted black, stator transients neglected; continuous grey, stator and rotor transients neglected

doi: 10.1049/iet-rpg:20070128

Table 3 Closed-loop controlled DFIG at synchronous speed

$\lambda = \sigma \pm j\omega$	f, Hz	ζ	Dominant states (contribution in %)	
full-order model				
−7421.3	0	1	stator electrical	$i_{qs} = 93$
−2940.4	0	1	stator electrical	$i_{ds} = 91$
−0.248 ± j313.48	49.89	0.001	rotor electrical	$e'_{qs} = 48$, $e'_{ds} = 47$
−2.82 ± j11.16	1.78	0.245	rotor mechanical	ω_r =46, $\theta_{tw} = 49$
−0.198	0	1	turbine mechanical	ω_t =91, ω_r =9
−423.23	0	1	q-axis current control	$\Phi_{iqr} = 94$
−214.30	0	1	d-axis current control	$\Phi_{idr} = 93$
−23.34	0	1	torque control	$\Phi_{T_e} = 96$
−9.95	0	1	reactive power control	$\Phi_{qs} = 99$
stator transients neglected				
−7.67 ± j306.03	48.71	0.025	rotor electrical	$e'_{qs} = 49$, $e'_{ds} = 48$
−2.82 ± j11.16	1.78	0.245	rotor mechanical	ω_r =46, $\theta_{tw} = 49$
−0.198	0	1	turbine mechanical	ω_t =91, ω_r =9
−405.80	0	1	q-axis current control	$\Phi_{iqr} = 97$
−209.40	0	1	d-axis current control	$\Phi_{idr} = 95$
−23.38	0	1	torque control	$\Phi_{T_e} = 97$
−9.95	0	1	reactive power control	$\Phi_{qs} = 99$
stator and rotor transients neglected				
−2.82 ± j11.16	1.78	0.245	rotor mechanical	ω_r =46, $\theta_{tw} = 49$
−0.198	0	1	turbine mechanical	ω_t =91, ω_r =9
−399.61	0	1	q-axis current control	$\Phi_{iqr} = 99$
−198.84	0	1	d-axis current control	$\Phi_{idr} = 99$
−23.34	0	1	Torque control	$\Phi_{T_e} = 97$
−9.95	0	1	reactive power control	$\Phi_{qs} = 99$

λ, eigenvalues, f, oscillation frequency; ζ, damping ratio. Operating point: $\omega_r = 1$ pu, $V_s = 1$ pu

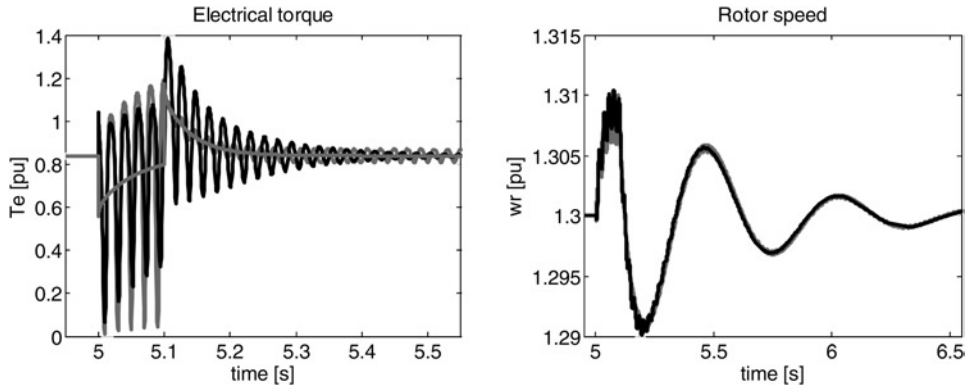

Figure 8 *Closed-loop DFIG at supersynchronous speed: response of the electrical torque and rotor speed to a drop in terminal voltage during 100 ms*
Dotted grey, full-order model; dash-dotted black, stator transients neglected; continuous grey, stator and rotor transients neglected

IET Renew. Power Gener., 2008, Vol. 2, No. 3, pp. 181–190

doi: 10.1049/iet-rpg:20070128

Table 4 Closed-loop controlled DFIG at supersynchronous speed

$\lambda = \sigma \pm j\omega$	f, Hz	ζ	Dominant states (contribution in %)	
full-order model				
−7424.9	0	1	stator electrical	$i_{qs} = 93$
−2941.8	0	1	stator electrical	$i_{ds} = 90$
−0.263 ± j313.24	49.85	0.001	rotor electrical	$e'_{qs} = 47$, $e'_{ds} = 46$
−2.16 ± j11.14	1.78	0.245	rotor mechanical	$\omega_r = 45$, $\theta_{tw} = 50$
−0.419	0	1	turbine-pitch mechanical	$\omega_t = 20$, $\Phi_{\omega_r} = 65$, $\beta = 12$
−0.347 ± j0.771	0.123	0.410	turbine-pitch mechanical	$\omega_t = 41$, $\Phi_{\omega_r} = 19$, $\beta = 36$
−422.93	0	1	q-axis current control	$\Phi_{iqr} = 93$
−214.85	0	1	d-axis current control	$\Phi_{idr} = 92$
−23.95	0	1	torque control	$\Phi_{T_e} = 99$
−9.95	0	1	reactive power control	$\Phi_{qs} = 99$
stator transients neglected				
−9.53 ± j302.47	48.14	0.032	rotor electrical	$e'_{qs} = 49$, $e'_{ds} = 47$
−2.16 ± j11.14	1.77	0.190	rotor mechanical	$\omega_r = 45$, $\theta_{tw} = 50$
−0.419	0	1	turbine mechanical	$\omega_t = 20$, $\Phi_{\omega_r} = 65$, $\beta = 12$
−0.347 ± j0.771	0.123	0.410	pitch control	$\omega_t = 41$, $\Phi_{\omega_r} = 19$, $\beta = 36$
−408.82	0	1	q-axis current control	$\Phi_{iqr} = 97$
−212.99	0	1	d-axis current control	$\Phi_{idr} = 93$
−24.00	0	1	torque control	$\Phi_{T_e} = 99$
−9.94	0	1	reactive power control	$\Phi_{qs} = 99$
stator and rotor transients neglected				
−2.16 ± j11.14	1.77	0.190	rotor mechanical	$\omega_r = 45$, $\theta_{tw} = 50$
−0.419	0	1	turbine mechanical	$\omega_t = 20$, $\Phi_{\omega_r} = 65$, $\beta = 12$
−0.347 ± j0.771	0.123	0.410	pitch control	$\omega_t = 41$, $\Phi_{\omega_r} = 19$, $\beta = 36$
−399.53	0	1	q-axis current control	$\Phi_{iqr} = 99$
−199.26	0	1	d-axis current control	$\Phi_{idr} = 99$
−23.95	0	1	torque control	$\Phi_{T_e} = 99$
−9.95	0	1	reactive power control	$\Phi_{qs} = 99$

λ, eigenvalues; f, oscillation frequency; ζ, damping ratio. Operating point: $\omega_r = 1.3$ pu, $V_s = 1$ pu

associated with the stator electrical transients. In power system stability studies, this stator mode can be ignored (i.e. stator variables can be assumed changing instantaneously) because it is associated with the stator dynamics irrespective of the operating point and is not in the bandwidth of interest. The other two modes have lower frequencies (0.5–10 Hz) and are associated with rotor electrical and mechanical dynamic characteristic. The degree of coupling between rotor mechanical and electrical dynamics as reflected by the participation factors depends on the operating point. It is highest when the induction generator is operating at near-synchronous speed, whereas at larger slip (positive and negative), electrical and mechanical parts tend to be decoupled [10, 13, 14]. It is useful at this point to point that the standard low-frequency electromechanical mode (0.1–2.5 Hz) in synchronous generator (zero slip) is coupled with participation from rotor speed, angle and rotor transient voltages. From these observations, it can be concluded that for the SCIG which operates at very small positive slip, a

simplified electromechanical model, whereby stator dynamics is neglected, is adequate.

For the closed-loop controlled DFIG, the controllers effectively separate the mechanical dynamics from the electrical ones and there is no electromechanical mode. As opposed to the open-loop control case discussed in [10, 13, 14], the oscillatory properties of the DFIG with closed-loop controls are not significantly sensitive to the rotor speed. The eigenvalue analysis showed that stator transients are associated with real eigenvalues far away from the imaginary axis in the left-half plane, whereas the high-frequency electrical mode is associated with the rotor electrical transients. As a result, the model of the DFIG with closed-loop controls can be further simplified by neglecting both stator and rotor electrical transients. The response of the simplified model is thus determined by the dynamics of the controllers and mechanical parts. For power system stability studies where the interest is in lower frequency oscillations, this is shown to be adequate from the observations of both time-domain and frequency-domain responses.

5 References

[1] PENA R., CLARE J.C., ASHER G.M.: 'Doubly fed induction generator using back-to-back PWM converters and its application to variable-speed wind-energy generation', *IEE Proc. Electr. Power Appl.*, 1996, **143**, (3), pp. 231–241

[2] MULLER S., DEICKE M., DONCKER R.W.D.: 'Adjustable speed generators for wind turbines based on doubly-fed induction machines and 4-quadrant IGBT converters linked to the rotor'. Proc. IEEE Ind. Appl. Conf., Rome, Italy, October 2000, pp. 2249–2254

[3] DATTA R., RANGANATHAN V.T.: 'Variable-speed wind power generation using doubly fed wound rotor induction machine – a comparison with alternative schemes', *IEEE Trans. Energy Convers.*, 2002, **17**, (3), pp. 414–421

[4] HOLDSWORTH L., WU X.G., EKANAYAKE J.B., JENKINS N.: 'Comparison of fixed speed and doubly-fed induction wind turbines during power system disturbances', *IEE Proc. Gener. Transm. Distrib.*, 2003, **150**, (3), pp. 343–352

[5] RODRIGUEZ J.M., FERNANDEZ J.L., BEATO D., *ET AL.*: 'Incidence on power system dynamics of high penetration of fixed speed and doubly fed wind energy systems: study of the Spanish case', *IEEE Trans. Power Syst.*, 2002, **17**, (4), pp. 1089–1095

[6] KOCH F.W., ERLICH I., SHEWAREGA F., BACHMANN U.: 'Dynamic interaction of large offshore wind farms with the electric power system'. Proc. Power Tech. Conf., Bologna, Italy, June 2003, pp. 1–7

[7] SLOOTWEG J.G., DE HAAN S.W.H., POLINDER H., KLING W.L.: 'General model for representing variable speed wind turbines in power system dynamics simulations', *IEEE Trans. Power Syst.*, 2003, **18**, (1), pp. 144–151

[8] MILLER N.W., PRICE W.W., SANCHEZ-GASCA J.J.: 'Dynamic modeling of GE 1.5 and 3.6 wind turbine-generators'. GE-Power Systems Energy Consulting'. Technical Report GE WTG Modeling-v3-0, 2003

[9] SAUER P., PAI M.: 'Power system dynamics and stability' (Prentice-Hall, 1998)

[10] KUNDUR P.: 'Power system stability and control' (McGraw-Hill, 1994)

[11] MEI F., PAL B.C.: 'Modelling and small-signal analysis of a grid connected doubly-fed induction generator'. Proc. IEEE Power Eng. Soc. General Meeting, San Francisco, USA, June 2005, pp. 2101–2108

[12] MEI F., PAL B.C.: 'Modal analysis of a grid connected doubly-fed induction generator'. Proc. Power Electronics, Machines and Drives Int. Conf., Dublin, Ireland, April 2006, pp. 611–615

[13] MEI F., PAL B.C.: 'Modal analysis of grid-connected doubly-fed induction generators', *IEEE Trans. Energy Convers.*, 2007, **22**, (3), pp. 728–736

[14] MEI F., PAL B.C.: 'Steady state and small signal dynamic behaviours of doubly fed asynchronous generators'. CIGRE Technical Brochure on Modeling and Dynamic Behaviour of Wind Generation as it relates to power system control and dynamic performance, 2007, vol. C4.601, (328), pp. A1–A18

doi: 10.1049/iet-rpg:20070128